Sputtering Thin Film NbTiN on Lithium Niobate Substrates

Linus Woodard and Indra Periwal
Mentors: Swaroop Kommera, Antonio Ricco, Don Gardner,
Prof. Amir Safavi-Naeini, Oliver Hitchcock, Kaveh Pezeshki

June 15, 2024

Abstract

In this work, we optimize physical sputtering parameters in the Lesker 2 sputtering system in the Stanford Nanofabrication Facility. We find that maximizing substrate bias, as well as setting chamber deposition pressure to 18 mTorr, allows for depositing 10 nm thin films of NbTiN with a critical transition temperature of 10.4 K. Additionally, we find that room temperature resistivity alone is not predictive of the transition temperature.

Contents

1 Introduction and Background

NbTiN thin films and lithium niobate (LN) have favorable properties which we wish to combine to advance the quality and robustness of nanomechanical resonators. Of particular interest in this project is maximizing the superconducting transition temperature, T_C, of NbTiN films grown on LN substrates.

1.1 Properties of NbTiN and Lithium Niobate

Superconducting materials have allowed for the development of many new quantum technologies including the advent of Josephson junctions [1], superconducting quantum interference devices (SQUIDs) [2], and superconducting nanowire single-photon detectors (SNSPDs) [3]. Superconductors are materials with zero DC resistance and are best evaluated according to the BCS theory which describes the flow of electricity according to cooper pairs – electrons pairs of opposite momentum which are bound together via phonon interactions – rather than typical electrons. Because there is no resistance, alternative properties are considered when evaluating the quality of superconducting materials. Phenomena such as the Meissner effect, the ability of the superconductor to completely shield internal magnetic fields, and magnetic levitation, typically prohibited under Earnshaw's theorem, are some of the hallmarks of superconducting materials. Additionally, the critical transition temperature can act as a figure of merit for superconducting materials. NbTiN is a superconducting metal with a high T_C of 16K when grown optimally [4, 5, 6]. Superconductors with such high T_C are exciting for two primary reasons. First, a high T_C means that modern dilution refrigerators can operate far below T_C where the effective quasiparticle density is extremely low. This is important when fabricating high Q resonators where quasiparticles become a major source of loss in the system. Resonator quality factors in superconducting resonators deteriorate quickly as the operating temperature approaches T_C, thus operating far below T_C where quasiparticle density is lowest allows for the suppression of these losses [7]. Second, with such high T_C it is possible to create devices that may operate at 4K, thereby eliminating the need for measurements in a dilution refrigerator. In addition to its high T_C, NbTiN has high kinetic inductance making it particularly attractive for quantum applications. Kinetic inductance is an inertial opposition to change in electromotive force (EMF) based on the finite mass of the charge carriers. This is in contrast to conventional inductance which is brought on by a change in magnetic flux opposing the EMF. The high kinetic inductance of NbTiN allows for tuning the effective inductance of circuit components via a magnetic field. Because resonance frequency is proportional to $1/\sqrt{LC}$, the ability to vary kinetic inductance via applied magnetic field translates directly into tenability of the resonance frequency in microwave resonators fabricated using NbTiN [8].

Lithium niobate (LN) is a piezo-electric material that also possesses χ^2 optical non-linearity making it a versatile material in both optics and mechanical applications. Nanomechanical systems have been proposed as a means of creating quantum-limited sensors, as well as for forming the basis of mechanical qubits [9, 10]. Lithium niobate nano-mechanical resonators have been integrated with microwave resonators in the LINQS group at Stanford. These devices demonstrate a step towards Dalton resolution mass sensors and are an important building block for quantum transduction [11].

For our project, we are particularly interested in the integration of NbTiN on LN to combine specific properties of each and improve nanomechanical devices. We are interested in the LN for its high piezoelectric coefficient, and we are interested in NbTiN for its high T_C, and kinetic inductance allowing for tunable microwave resonators. Because ultimately the NbTiN will be deposited on an LN phononic crystal, we focus the scope of our project on NbTiN films of approximately 10 nm, as thicker films begin to disrupt the mechanical properties of the crystals.

1.2 Project Goals

This project aimed to optimize the sputtering deposition process for achieving high critical transition temperature T_C NbTiN thin films on Lithium Niobate (LN) substrates using a Lesker2 Sputter System. To this end, we employed a design of experiment (DoE) approach to systematically explore the parameter space for NbTiN deposition within the Lesker2 system. Following deposition, each sample underwent a characterization process to assess its electronic and film properties. Electrical characterization utilized the Van der Pauw four-point probe method to determine the residual resistivity ratio (RRR), while T_C was directly measured in a cryogenic environment. Lithium niobate substrates were provided by the LINQS group, and are comprised of 300 nm of LN on SiO_2.

2 Benefits to the SNF Community

High-quality NbTiN films may be purchased from third-party vendors, however, this limits the flexibility of substrates available and precludes the use of liftoff processes which are crucial for some processes where harsh etching conditions may adversely affect existing structures. This project will benefit the SNF community by

- Creating a generally available SOP for growing high-quality NbTiN films in the Lesker 2 Sputter tool.
- Helping to understand the possibilities and limitations of growing NbTiN on substrates other than Si.
- Identifying key parameters to monitor for identifying process drift over time.
- Developing a robust measurement protocol for superconducting films that can be utilized by other SNF users.

3 Fabrication and Process Development

To test the T_C of NbTiN sputtering with different sputtering parameters we develop a process flow to streamline testing. We first sputter NbTiN onto an LN substrate. We vary the parameters of the sputtering process and this makes up our design of the experiment. Next, we design and pattern the films into Van der Pauw squares so we can do characterization at room temperature. Finally, for films that behave the way we would expect at room temperature, we package them and measure their T_C in a dilution refrigerator. The idea here is that we can optimize the sputtering parameters to have the highest T_C possible.

3.1 Reactive Magnetron Co-deposition Sputtering

Sputtering is a deposition technique. Inside an ultra-high vacuum chamber are targets of the material we want to sputter and a substrate that is rotating above it. The target is the cathode and the substrate is the anode. There is a magnet below the targets which generates an electric field between the anode and the cathode. A gas plasma is excited inside of the chamber.

The ions in the plasma are attracted to the cathode by an applied DC voltage to the target materials. The energy of the incident ions is transferred to the atom surface of the target by atomic collisions, for us the is the Ar+ ions. This then ejects atoms from the surface this only happens if the energy of the ions is larger than the binding energy of the targets, in our case the Nb and

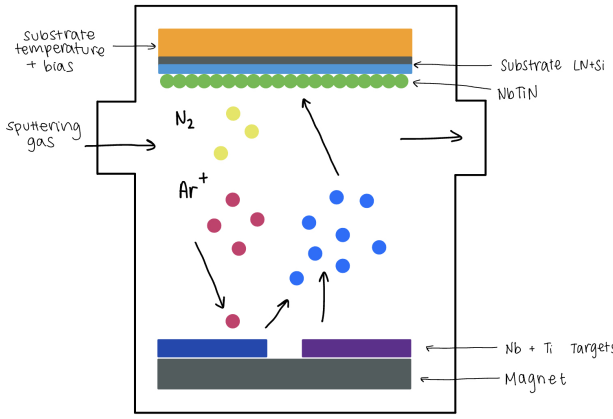

(a) Diagram of the reactive gas co-deposition of Nb and Ti onto LN. Ar+ and N_2 gas are flowed into the chamber. Nb and Ti atoms are ejected from the target and deposited onto the LN.

(b) Plasma in the chamber and Nb and Ti targets, Lesker2

Figure 1: Dilution Refrigerator Measurements

Ti. Typically for magnetron sputtering, or sputtering with the use of a magnet the electrons in the plasma are confined in a region close to the surface of the target. The rate of sputtering is thus increased. The Nb and Ti atoms go towards the substrate. We also introduce nitrogen gas into the chamber and let it react with the niobium atoms as it comes off of the targets. This is known as reactive gas sputtering. The Nb and N_2 gas form NbN which is then deposited onto the substrate along with the Ti [12].

For our project, we wanted to grow films that were approximately 10 - 20 nm in thickness. To characterize our deposition rate we compare the thickness to the deposition time. To get thickness measurement we do a Sharpie test. To do this we utilize a method where we have a witness chip with every LN chip that we deposit on. This witness chip is how we characterize film stress measurements as well as thickness. We add a sharpie mark to the witness silicon chip. This ensures that there is a section of the chip that does not have any film deposited on it/the sharpie mark can be cleaned off revealing the substrate underneath. After deposition, we sonicate the chip in acetone and IPA to remove the sharpie mark and then do profilometry to look at the thickness of the film.

Many parameters affect the deposited film, the power applied to the targets, the Ar flow rate, the N_2 flow rate, substrate temperature, and substrate bias. When determining which parameters to change we think about what is physically happening in the deposition chamber. The first parameters that we changed were the Nb target power and the ratio of N_2 gas to Ar gas that is in the chamber. If there is more power on the Nb target physically we expect that there will be more Nb atoms coming off of the surface. In increasing the N_2 gas ratio we can think of this as having more N_2 for the Nb to react with thus increasing the amount of Nb in the grown film. With more reactive gas there is an increased chance of a sputtered atom colliding into the N_2 and forming a molecule before reaching the substrate.

The next set of parameters that we looked at was the DC substrate bias power and the total chamber pressure. The substrate bias applies an electric voltage to the substrate which affects the energy of the bombarding ions and film properties. Physically we can think of this as adding a force that pulls the sputtered atoms towards the substrate and compacts the film. Changing the total

chamber pressure affects the mean free path of the sputtered atoms and reactive gas molecules.

The last parameter that we looked at was heating the substrate. This changes the mobility of atoms on the substrate surface, higher temperature increases atomic mobility and increases the surface diffusion coefficient allowing for reordering of the film.

3.2 Pattern

To uniformly characterize the electrical properties of deposited films on LN chips, independent of chip variations, we utilize the Van der Pauw pattern for measurements. This pattern is fabricated using photolithography.

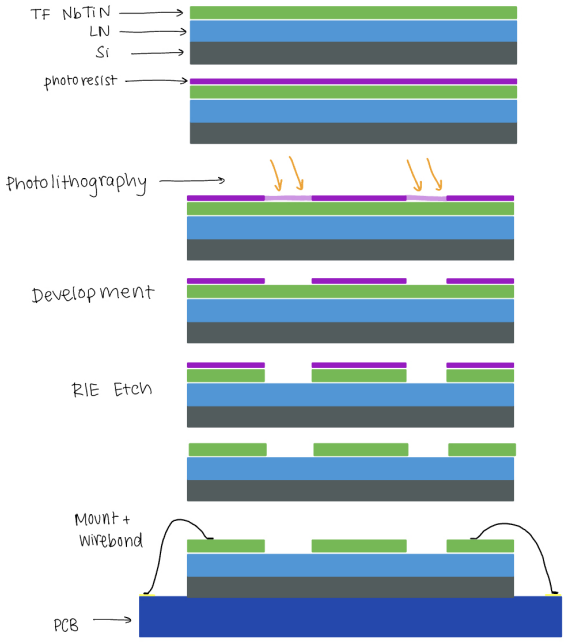

(a) Diagram of the patterning process steps.

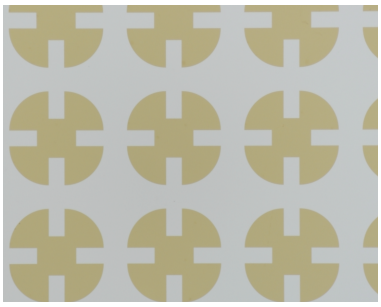

(b) Pattern

Figure 2: Patterning process and results

1. We start by cleaning chips after NbTiN is deposited on them.
2. A dehydration bake at 150 C removes moisture and improves adhesion for the photoresist (SPR-3612). The resist is then spin-coated at 5500 rpm with a 45-second ramp to 1500 rpm, resulting in a 1 um thick layer. This is followed by a 1-minute bake at 90 C for further curing.
3. Next we use the Heidelberg2 maskless aligner for direct write photolithography. We expose our pattern in optical autofocus mode since we are using chips. We use a dose value of 105 mJ/cm2 and a de-focus value of -2.
4. Following exposure, the resist is developed in MF-26A for 18 seconds and rinsed with DI water for 30 seconds each. The developed pattern is then inspected under an optical microscope.

5. Next we use the Oxford REI Plasma Pro-80 using the LINQS NbTiN-CF4 recipe. The total process is
   (a) Chamber Clean: 5 min 100 mtorr 50 sccm O2 300 W
   (b) Chamber Seasoning: 4 min 100 mtorr, 210 W, 2 sccm O2, 20 sccm CF4
   (c) Etch: 30 s 100 mtorr, 210 W, 2 sccm O2, 20 sccm CF4
   (d) Resist Strip: 30 sec, 30 mtorr, 100 W, 50 sccm O2.
6. After the etch we check that all the NbTiN has been removed.
7. The chip is bonded to a PCB using varnish, followed by a 45-minute bake at 50°C to ensure complete curing.
8. Aluminum wires are attached between the PCB electrodes and the four pads of the Van der Pauw structure using a West Bond 7476E Wedge-Wedge Wire Bonder.

3.3 Package

Following wire bonding, the PCB assembly is integrated into a dedicated housing for electrical characterization measurements within the dilution refrigerator. The PCB is securely fastened into the copper housing using screws. A screw-on lid is then attached to the housing to provide physical protection for the delicate sample and wire bonds.

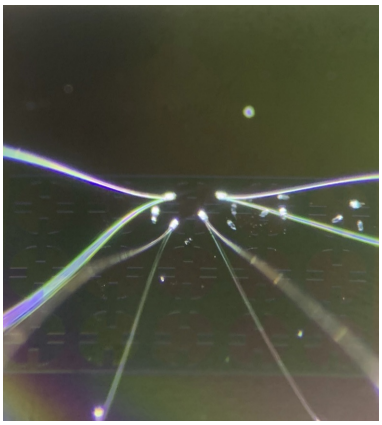

(a) Image of the wire bonds on the Van der Pauw pattern.

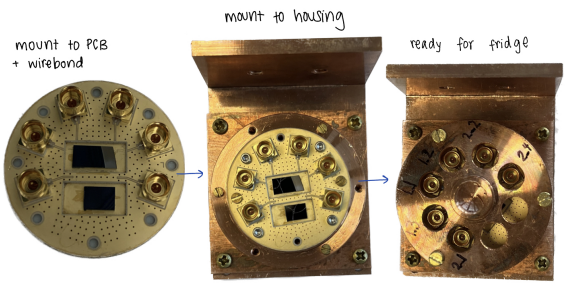

(b) Steps from wire-bonding to packaging for the dilution fridge

Figure 3: Patterning process and results

The wire bonds must form a strong and low-resistance connection between the aluminum wires, the NbTiN thin film pads on the chip, and the PCB electrodes. Strong adhesion of the wire bonds to both the film and PCB is essential to withstand the physical stresses encountered during handling and thermal cycling, especially the extremely low temperatures within the dilution refrigerator.

3.4 Characterize

Before sample mounting and wire bonding, we performed essential characterization measurements to assess film properties. We utilized a DekTak profilometer (located in either the SNSF or SMF cleanroom) to determine film thickness using a step height measurement on a dedicated witness chip. This also helps us to determine the deposition rate for our different deposition recipes.

A DekTak profilometer utilizes a fine diamond-tipped stylus to precisely scan the surface of a sample. As the sample stage precisely moves the material underneath, the stylus maintains a constant, gentle force against the surface. By meticulously tracking the vertical movements of the stylus, the DekTak can create a detailed profile of the sample's topography. This allows for precise measurement of features like thin film thickness, step heights between different material layers, and even surface roughness.

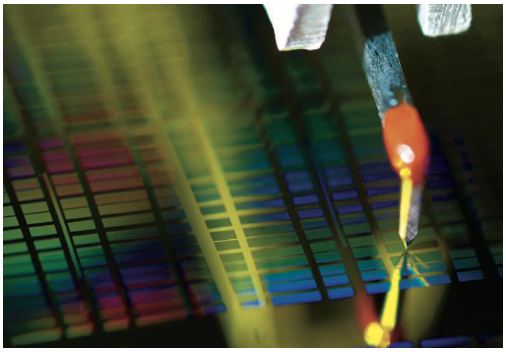

(a) Close-up image of the Dektak tip

(b) Image of the Dektak Profilometer

Figure 4: Thickness Characterization

We employed atomic force microscopy (AFM) on one sample to evaluate its surface morphology. The results confirmed a characteristic surface roughness typical of sputtered thin films. Given the consistency with expected behavior and reliable thickness data obtained from profilometry, further AFM measurements were deemed unnecessary.

3.5 Measurement

Following deposition, each sample goes through a two-part characterization process to assess its electrical properties. First, room temperature resistance measurements were performed using a micromanipulator6000. This initial measurement provided a basic understanding of the sample's conductivity. T_C measurements were conducted using a dilution refrigerator. For these measurements, the sample housing was mounted directly within the cryogenic environment of the refrigerator. Additionally, a lock-in amplifier setup, identical to the one employed for low-temperature measurements, was utilized to characterize the room-temperature resistivity with enhanced precision.

Fabrication of a functional resonator on the LN substrate proved impractical. This is because LN exhibits piezoelectricity, which translates mechanical vibrations into electrical signals and vice versa. The presence of a resonator on a piezoelectric substrate would lead to unwanted electrical noise due to these inherent vibrations. This necessitates exploring alternative substrate materials that lack piezoelectricity for future resonator development.

4 Experimental Methods

To ensure consistency across measurements, we developed a set of experimental methods used to characterize all films in this project. These methods are optimized to utilize the resources from SNF as well as in our labs to produce high-quality data about the properties of our films. In

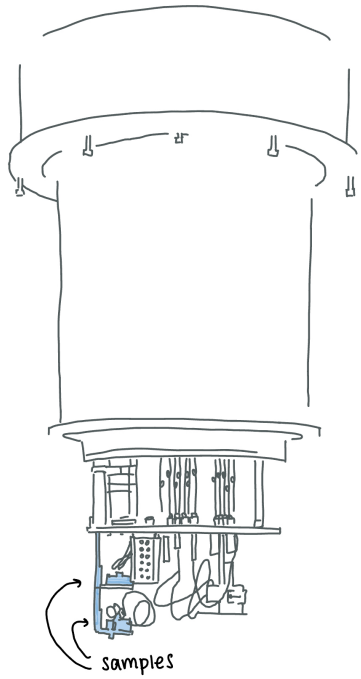

(a) Sketch of the dilution refrigerator

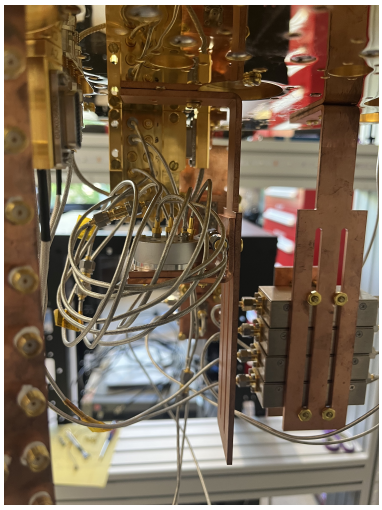

(b) Image of the housing mounted inside the dilution refrigerator.

Figure 5: Dilution Refrigerator Measurements

designing our experiments, we attempt to maximize the efficiency of our testing procedures to produce meaningful data over ten weeks.

4.1 Design of Experiment

To efficiency converge on optimal sputtering parameters, we chose to employ a design of experiments (DOE). In a sputtering deposition, there is a large parameter space to choose from including the power to each target, reactive gas partial pressures, total chamber pressure, substrate bias, and substrate temperature. This does not include other techniques having to do with depositing interfacial layers for lattice matching or other pre/post depositions steps that may change the quality of the films. Based on the relevant variables explored in Ref. [6, 4], as well as work previously carried out for NbN by Maksymowych et al. in a previous E241 project, we chose to explore Nb target power, and N_2 partial pressure while holding all other variables fixed in our initial DOE. DOE Parameters can be seen in Fig 6.

From this DOE we were able to draw some conclusions about process parameters and deposition rates, as well as the resulting film resistivity. However, all films grown from the parameters in this DOE had high and non-uniform contact resistance at the interface with wire bonds. The high contact resistance hindered our ability to use the T_C measurement setup which will be discussed in more detail in the next section, and for this reason, we have no T_C data for this initial batch of samples. In addition, samples from the initial DOE displayed non-ohmic behavior during room temperature resistivity characterization leading us to believe these films were of low quality, and likely not the high T_C superconductors that we were hoping for.

In an attempt to find DOE parameters that were effective at varying T_C, we moved on to study parameters affecting the physics of the deposition. Namely, we varied DC substrate bias power, as

Sample Name	Nb Power (W)	N2 ratio (%)
NLN01	150	7.5
NLN02	200	15
NLN03	150	15
NLN04	200	7.5

Figure 6: Initial DOE parameters. While these parameters are varied, the other sputter parameters are constant: P_{ch}: 8 mTorr, Ti Power: 200 W, Substrate bias: 0 W, Substrate temperature: 20 C.

well as total chamber pressure. In addition to these parameters, the N_2 ratio was revisited, as this appears to be one of the important factors in optimizing T_C of NbTiN films grown with reactive sputtering [6, 4]. Our second DOE can be seen in Fig. 7.

Sample Name	N2 ratio (%)	Pcap (mTorr)	Substrate Bias (W)
NLN11	7.5	15	70
NLN12	7.5	15	100
NLN13	7.5	15	85
NLN14	7.5	18	100
NLN15	7.5	5	100
NLN16	7.5	10	100
NLN17	15	15	100
NLN18	25	15	100

Figure 7: Second DOE. Pcap is the pressure set in the recipe and controls the feedback loop to a valve in the chamber thus regulating pressure. It is not the true chamber pressure during deposition which tends to settle at approximately half this value. During these depositions other deposition parameters are held constant: Nb Power: 150 W, Ti Power: 200 W, Substrate temperature: 20 C.

4.2 T_C Measurements

Direct T_C, measurements of many different films were the ultimate goal of this project, as a thorough investigation of film quality through direct measurement has yet to be conducted for Lesker2 NbTiN. The limiting factor on these types of measurements is that to date, they have been conducted by using a dilution refrigerator to reach T_C. Dilution fridges are somewhat overkill for simple measures of T_C as they take approximately two days to cool down, two days to warm up, and reach millikelvin temperatures which are far below the T_C of interest for NbTiN. Additionally, these systems are designed to stay cold for long periods, not for fast cycling. This is to say that, the limiting factor in this work was the time required to cool samples down to reach T_C. We employed a few strategies in this work which increase the number of samples that may be measured in a single cool down, and have some suggested ideas for improving measurement times in the future work section.

To measure T_C, we mount the samples to PCBs and wire bond to the connectors as discussed in section 3.3. We mount these samples on copper brackets to the mixing plate of a Blue Fors dilution refrigerator. The number of T_C measurements we can get in a single cooldown is limited

by the availability of measurement electronics. We only had access to enough equipment to build one measurement setup (to be discussed shortly), thus limiting us to two T_C measurements per cool down – one sample on cool down and one sample on warm up. The samples are connected to separate DC input/output lines, making it easy to change which device is connected between cool down and warm up. In theory, it is possible to measure three samples per cool down, limited by the 12 DC lines that go to the mix plate. This would mandate measuring on cool down, measuring on warm-up, then cooling down again once the T_C of the second sample is reached, and measuring the third sample on the subsequent cooldown. The fridges cycle fairly quickly between 20 K and 4 K making this scheme a possibility and we recommend taking this approach for anyone attempting to take large volumes of T_C measurements in the future.

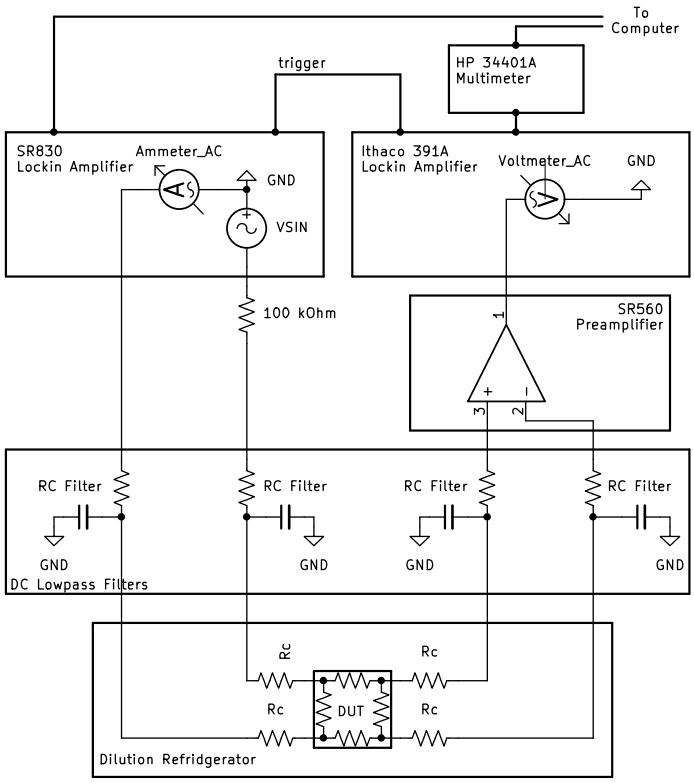

Figure 8: Lumped element diagram of the cryogenic wiring setup. Thin lines represent wires that are part of the measurement, while thicker lines indicate digital communication lines.

We now turn to the measurement setup. We conduct a four-point probe measurement using one lock-in to measure voltage, and another lock-in to measure current. Cooling power on the mixing plate of a dilution fridge is extremely limited, thus when conducting any measurement that will discharge power it is important to be thoughtful about the amount of power that is sent through the DUT. With this in mind, we would like to probe the sample with small currents that will not discharge very much power. With small probing currents, we will need to measure small voltage changes. This is best achieved through the use of lock-in amplifiers, which send an alternating signal and then amplify responses of the same frequency. To drive and measure current, we use an SR830 lock-in amplifier. At the output of the lock-in, we add a 100 kΩ resistor. This resistor is meant to stabilize the current through the system so that the lock-in range is not overloaded when the wire bonds and film become superconducting. The drive signal then passes through DC lowpass filters

and to one pad of the van der Pauw clover in the dilution fridge. From a pad on the same side, the current is returned, through more lowpass filters, to the SR830 where the current is measured. The two remaining pads of the van der Pauw clover are connected to DC lines and pass through DC lowpass filters. The voltage difference between these two pads is taken using an SR560 low-noise preamplifier, and the resulting signal is set to an Ithaco 391A lock-in amplifier. The 391A and SR830 are triggered together ensuring that signals at the same frequency are amplified. The 391A does not have an internal ADC and thus cannot connect directly to a computer. This mandates sending the aux out of the 391A to an HP 34401A multimeter which can then be connected to a computer for data logging. The low pass filters on the DC lines limit the operating frequency of the lock-in amplifiers. To tune the operating frequency, we look at the phase response of the measured current. As long as the transfer function is purely resistive, the current response should be in phase with the probe signal ($\theta = 0, \pi$). However, as the frequency is increased, the RC low pass filters begin to interact with the signal, thus adding a capacitive response to the transfer function. This manifests as a phase response tending toward $\pi/2$. To set the frequency of the lock-in we increase the frequency until we begin to see a change in phase response, then lower the frequency just until the phase response is purely resistive. A schematic of the measurement setup can be seen in figure 8.

The current and voltage data from the SR830 and Ithaco 391A are logged with time stamps to a computer. This data is then aligned with the temperate log from the Blue Fors to find the behavior of resistance with temperature.

4.3 Micromanipulator Measurements

For characterizing the room temperature resistivity of our films, we utilized the Micromanipulator6000 in the SNF facilities. This tool has four tungsten probes each connected to a micrometer three-axis stage. This allows for fine control over probe placement on test pads as small as 100 μm in diameter comfortably.

Our films were patterned with the standard van der Pauw clovers (Fig 9) which significantly reduce the effects of contact resistance, and create a well-defined effective square over which to measure [13]. Four-point van der Pauw measurements work by passing current along one side of a rectangular sample and measuring the induced voltage along the other edge. A diagram of a typical four-point measurement is shown in Fig 9. For non-uniform samples the formula to extract the sheet resistivity for such measurements is

$$e^{-\pi R_V/R_S} + e^{-\pi R_H/R_S} = 1 \tag{1}$$

where R_V and R_H are the measured resistances across the vertical and horizontal directions of the sample. In general, this formula does not have an analytic solution for R_S. However, in the case of uniform films and measurements along the edges of a well-defined square, the equation simplifies to

$$R_S = \frac{\pi R}{\ln 2}. \tag{2}$$

The sheet resistance R_S or a film is related to the material resistivity, ρ (which is the more fundamental property) by

$$\rho = R_S \cdot d \tag{3}$$

where d is the thickness of the film.

Using the micromanipulator6000 we measured the sheet resistance of our samples. The two recipes used for this are the "van der Pauw", which uses a mixed configuration of current source and voltage measurement probes but sweeps the current during the measurement, and "van der Pauw Non-Uniform", which reassigns the current sources and voltage measurements to average all combinations but uses a fixed current. In both recipes, the geometric factor of $\pi/\ln 2$ is accounted for in the software.

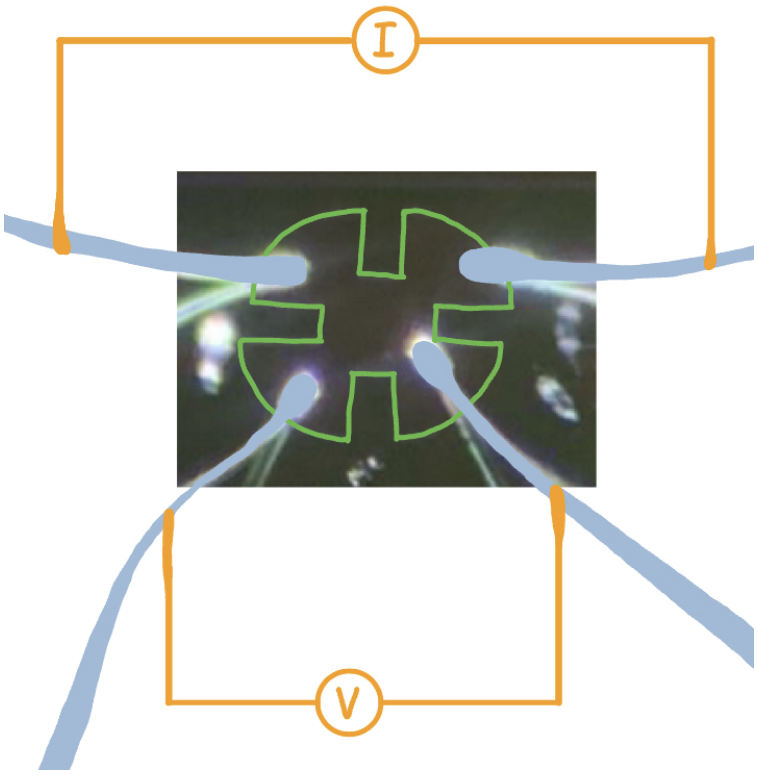

Figure 9: Outline of our van der Pauw clover test structure and the connections to current source and volt meter.

4.4 Profilometry Measurements

Our project aims to investigate the properties of NbTiN films that are 10 nm thick. Additionally, the T_C of superconducting films becomes highly dependent on film thickness when the thickness approaches the coherence length of the films, as is the case for our system [5, 6]. To measure the thickness of our films, employ sharpie liftoff and profilometry of a witness sample that is deposited concurrently with our LN sample.

Profilometry measurements were primarily taken on the Dektak in the nano-patterning cleanroom.

4.5 Flexus Film Stress Measurements

Residual film stress in sputtered materials can be an excellent indicator of the film properties. In NbTin large compressive stress is indicative of high-quality films [14]. To measure Stress we use the Flexus 2320 Stress Tester in SNF.

The operating principle of the Flexus is sweeping a laser beam along the diameter of a wafer, and simultaneously tuning the position of a photodiode to maintain the maximal reflected intensity. From this procedure, the curvature of the wafer can be calculated, and subsequently the film stress. The relation is outlined by the well-known Stoney equation

$$\sigma = \frac{1}{6}\frac{E}{(1-\nu)}\frac{t_s^2}{t_f}\left(\frac{1}{R_f - R_s}\right)$$

where E is Young's modulus of the wafer, ν is Poisson's ratio, t_s is the substrate thickness, t_f is the film thickness, and R_f, R_s are the radii of curvature both before and after film deposition.

5 Results

5.1 Optimal parameters for T_C

Our measurements of T_C while sweeping substrate bias yielded a strong correlation. Figure 10 displays the superconducting phase transition of three samples deposited at different substrate bias powers. From the plot, it is clear that T_C increased when films were deposited at high substrate bias powers. Samples deposited at 85 W and 100 W bias powers were cycled through their transition temperatures, allowing us to collect data both on warm-up and cool-down. Due to imperfect thermalization between the thermometer and the sample, there is a slight time delay between the temperature reported by the thermometer and the true temperature of the sample. This means that data collected on cooldown indicates the lower bound for T_C, while data collected on warm-up indicates an upper bound for T_C. The sample deposited at 70 W substrate bias power was only measured on cool down, and thus the data displayed here should be considered a lower bound. Additionally, this sample has some anomalous behavior. Notice that there is a second hump in the drop resistivity drop, and subsequently, the sheet resistance drops briefly by several orders of magnitude below its ultimate steady state. We have considered that this behavior may be due to the wire bonds superconducting phase transition, but this hypothesis does not align with the T_C reported for aluminum of 1.2 K. While from the trend it seems that further increasing the substrate bias will continue to increase the T_C of our films, we are limited by tool capability here as the Lesker2 Sputter System has a maximum substrate bias power of 100 W.

Measurements of T_C for samples deposited under various process chamber pressures also reveal a positive correlation for the domain studied here. Figure 11a shows that for sufficiently high chamber pressure there is little difference in the resulting Tc. However, when moving away from this optimal range there is a sharp drop-off in Tc. It is worth noting that in the Lesker2 sputter system, the amount of nitrogen in the chamber is controlled as a percentage of the total chamber gas. This means that by increasing chamber pressure, the nitrogen partial pressure also increases. This indicates that the increase in T_C witnessed may be a joint effect of the difference in film morphology due to the shorter mean free path of sputtered ions at higher pressure, as well as a change in stoichiometry due to greater nitrogen incorporation in the films.

5.2 T_C correlation with ρ_{RT}

One aim of this project was to see if there were correlations between room temperature film properties and T_C. Such metrics would be extremely useful as they would allow SNF users to conduct a quick test of the deposited films at room temperature before moving ahead with a costly cooldown of their devices. Unfortunately, we found that room temperature resistivity measurements are not

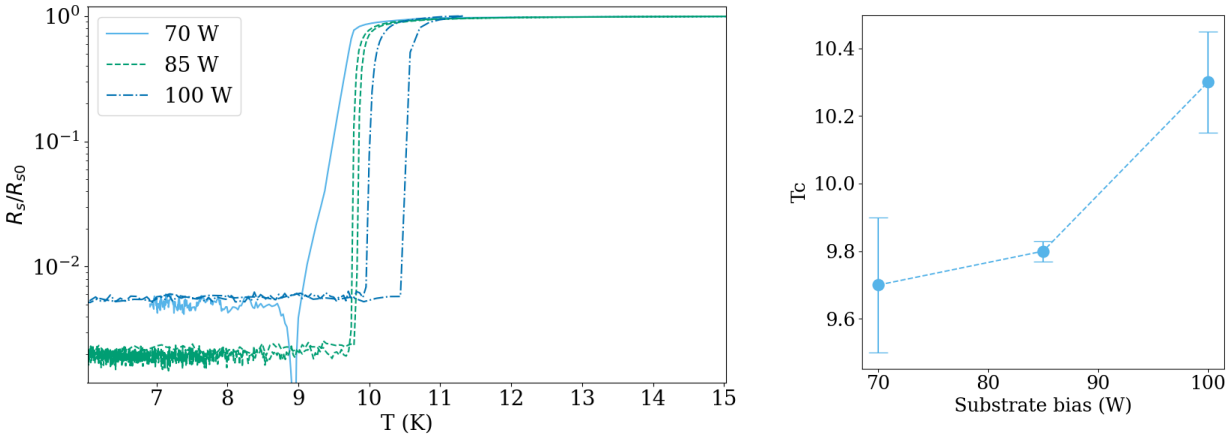

Figure 10: (left) Resistance vs temperature. The three curves plotted are samples deposited at different DC substrate bias power conditions, with all other deposition variables held constant. The hysteresis seen in the plot is due to imperfect thermalization between the sample and the thermometer. (right) Trend in T_C with substrate bias. Error is calculated based on the spread of T_C measured from the hysteresis, or in cases without hysteresis, based on the width of the transition.

predictive of films T_C. A sample of measured T_C vs ρ_{RT} can be seen in figure 11b. BCH theory and other studies have shown that these metrics are not necessarily correlated, and this result will be discussed further in the next section.

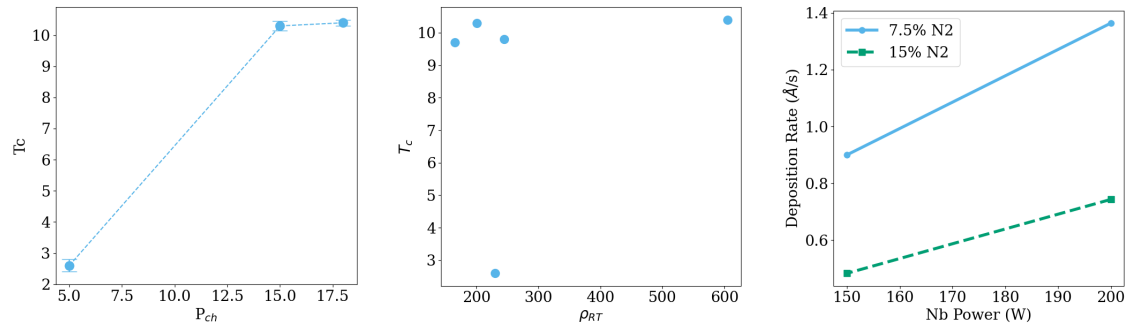

(a) (b) (c)

Figure 11: (a) T_C vs process chamber pressure during deposition. Error in measurements is calculated from hysteresis of the R_S vs T curve. (b) T_C vs ρ_{RT}. The scatter plot shows no discernible correlation between these two metrics. (c) Deposition rate vs Nb target power at different chamber atmospheres.

5.3 Deposition rates

We find, perhaps unsurprisingly, that deposition rate and target power are positively correlated. More surprisingly, we find that deposition rate and N_2 percentage are negatively correlated. It is likely that when the ratio of N_2 in the chamber is optimal for growing stoichiometric films, the deposition rate increases. Considering that the physics of the ion deposition seems critical to producing high Tc films, monitoring the deposition rate of the recipe is an easy way to identify process drifts that may be detrimental to film quality. Figure 11c displays the correlations between these two parameters and deposition rate.

5.4 Film Stress

We conducted film stress measurements over several of the samples, however, we failed to see notable changes in the wafer bow before and after deposition. Because these measurements required deposition on an entire wafer during each deposition, they were discontinued after several depositions finding that there was not a meaningful change in bow after deposition.

6 Discussion

This study explored how deposition parameters influence the superconducting transition temperature T_C of NbTiN thin films on LN. The findings align with established principles for NbTiN films. Both increased substrate bias power and maintaining an optimal chamber pressure during deposition led to higher Tc. Higher bias likely creates denser films, while optimal pressure ensures proper nitrogen incorporation, both crucial for high T_C.

An interesting finding was the negative correlation between deposition rate and N_2 percentage. While the mechanism behind this needs further investigation, it highlights the complex interplay between deposition conditions and NbTiN film properties.

The relationship between a material's Tc and room temperature (RT) resistivity isn't always straightforward, especially for NbTiN and other type-II superconductors. While both properties influence conductivity, they don't directly reflect the superconductivity mechanism.

Superconductivity arises from Cooper pairs – bound electron states with zero electrical resistance. The BCS theory attributes this to electron-phonon coupling mediated by lattice vibrations (phonons). RT resistivity, however, is influenced by various scattering mechanisms that may not significantly impact Cooper pair formation at T_C, leading to a potential decoupling between the two properties.

For NbTiN, deviations from the optimal stoichiometry can affect both RT resistivity and T_C. However, the influence on T_C is often more complex. Excess nitrogen can introduce states that suppress superconductivity, but might also enhance phonon coupling, potentially leading to a non-monotonic relationship between T_C and RT resistivity.

There is a striking similarity in the observed N_2 optimum and that observed by Pratap et al. [4]/we chose N_2 ratios based on previous work and the work presented in [4].

There are a few shortcomings of our work that could have been improved. Variations in film thickness across samples can affect electrical properties. Optimizing deposition processes to achieve better uniformity is crucial. The base pressure in the sputter chamber can influence film purity and quality. Further investigation into the optimal base pressure might be beneficial. Precise stoichiometry control is essential for high-quality NbTiN films. Refining our understanding of the deposition process and its impact on stoichiometry is necessary.

7 Conclusion and Future Work

This project developed a sputtering recipe for NbTiN thin films achieving a T_C of 10 K. Higher substrate bias power (85 W and 100 W) led to increased T_C compared to 70 W, suggesting further exploration beyond the system's 100 W limit might be beneficial. However, the anomalous double transition behavior observed in the 70 W sample requires further investigation.

Chamber pressure also impacted T_C. A positive correlation was found within a specific pressure range, plateauing at higher pressures and dropping significantly at lower ones. Since N_2 content

tracks with pressure in the Lesker2 system, this suggests a dual effect: altered film morphology due to shorter mean free path and potential stoichiometry changes from increased N incorporation.

While a rapid room-temperature screening method for T_C was desired, no correlation between room-temperature resistivity and T_C was observed. This aligns with the existing theory.

As expected, the deposition rate increased with target power. Interestingly, it showed a negative correlation with N_2 percentage, suggesting an optimal N2 ratio for achieving both stoichiometric films and higher deposition rates. Monitoring deposition rate can be a useful tool to identify potential process drifts impacting film quality.

Future efforts will focus on the precise characterization of film composition and the NbTiN-LN interface. Raman spectroscopy will determine stoichiometry, while XRR and XPS will provide detailed interface information.

To further optimize film properties, we'll investigate the influence of film thickness on both room-temperature resistivity and T_C. Additionally, building on prior work and that of Nate Newman, we propose exploring the effects of the pre-deposited Nb layer on the interface and electrical characteristics and substrate temperature variation on superconducting properties. Oxygen filter on the Argon line for finer oxygen content control and potentially improved T_C. Minimizing oxygen contamination is crucial to avoid Nb oxide formation that can degrade superconductivity. We'll closely monitor gas composition to ensure a pristine deposition environment.

By implementing these advancements, we aim to achieve a deeper understanding of factors influencing NbTiN film properties and ultimately guide the development of high-performance NbTiN devices.

8 Acknowledgements

IP and LW would like to thank Debbie Senesky and Sergio Cordero for making this class possible and our staff mentors, Swaroop Kommera, Don Gardner, and Antonio Ricco for all their support and guidance. IP and LW would also like to acknowledge Amir Safavi-Naeini for project guidance, Oliver Hitchcok and Samuel Gyger for additional guidance, and Kaveh Pezeshki for support with the cryogenic measurement setup, contributing personal test equipment, and insight on superconductivity theory.

References

[1] Aki Ruhtinas and Ilari J. Maasilta. Highly tunable nbtin josephson junctions fabricated with focused helium ion beam, 2023.

[2] A. Lupaşcu, C. J. P. M. Harmans, and J. E. Mooij. Quantum state detection of a superconducting flux qubit using a dc-squid in the inductive mode. *Physical Review B*, 71(18), May 2005.

[3] Jin Chang, Johannes W. N. Los, Ronan Gourgues, Stephan Steinhauer, S. N. Dorenbos, Silvania F. Pereira, H. Paul Urbach, Val Zwiller, and Iman Esmaeil Zadeh. Efficient mid-infrared single-photon detection using superconducting nbtin nanowires with high time resolution in a gifford-mcmahon cryocooler. *Photon. Res.*, 10(4):1063–1070, Apr 2022.

[4] Pratiksha Pratap, Laxmipriya Nanda, Kartik Senapati, R P Aloysius, and Venugopal Achanta. Optimization of the superconducting properties of nbtin thin films by variation of the n2 partial

pressure during sputter deposition. *Superconductor Science and Technology*, 36(8):085017, jul 2023.

[5] Lei Yu, Nathan Newman, and John M. Rowell. Measurement of the coherence length of sputtered nb0.62ti0.38n thin films. *IEEE Transactions on Applied Superconductivity*, 12(2):1795–1798, June 2002.

[6] Lei Yu, R.K. Singh, Hongxue Liu, S.Y. Wu, R. Hu, D. Durand, J. Bulman, J.M. Rowell, and N. Newman. Fabrication of niobium titanium nitride thin films with high superconducting transition temperatures and short penetration lengths. *IEEE Transactions on Applied Superconductivity*, 15(1):44–48, 2005.

[7] P.B. Fischer and G. Catelani. Nonequilibrium quasiparticle distribution in superconducting resonators: An analytical approach. *Phys. Rev. Appl.*, 19:054087, May 2023.

[8] Mingrui Xu, Xu Han, Wei Fu, Chang-Ling Zou, and Hong X. Tang. Frequency-tunable high-Q superconducting resonators via wireless control of nonlinear kinetic inductance. *Applied Physics Letters*, 114(19):192601, 05 2019.

[9] F. Pistolesi, A. N. Cleland, and A. Bachtold. Proposal for a nanomechanical qubit. *Phys. Rev. X*, 11:031027, Aug 2021.

[10] Jeffrey C. Taylor, Eric Chatterjee, William F. Kindel, Daniel Soh, and Matt Eichenfield. Reconfigurable quantum phononic circuits via piezo-acoustomechanical interactions. *npj Quantum Information*, 8(1):19, Feb 2022.

[11] Sultan Malik, Wentao Jiang, Felix M. Mayor, Takuma Makihara, and Amir H. Safavi-Naeini. Flexible integration of gigahertz nanomechanical resonators with a superconducting microwave resonator using a bonded flip-chip method, 2023.

[12] Reactive Sputtering - an overview | ScienceDirect Topics.

[13] L.J. van der Pauw. A method of measuring specific resistivity and hall effect of discs of arbitrary shape. *Philips Res. Repts*, 13(1):1–9, 1958.

[14] T. Matsunaga, H. Maezawa, and T. Noguchi. Characterization of nbtin thin films prepared by reactive dc-magnetron sputtering. *IEEE Transactions on Applied Superconductivity*, 13(2):3284–3287, 2003.